AFRL-AFOSR-UK-TR-2022-0131

High Average Power Difference-Frequency Generation in the Mid-Infrared

Robbie Murray
IMPERIAL COLLEGE OF SCIENCE TECHNOLOGY & MEDICINE
EXHIBITION RD
LONDON, ,
GB

09/20/2022
Final Technical Report

DISTRIBUTION A: Distribution approved for public release.

Air Force Research Laboratory
Air Force Office of Scientific Research
European Office of Aerospace Research and Development
Unit 4515 Box 14, APO AE 09421

REPORT DOCUMENTATION PAGE

PLEASE DO NOT RETURN YOUR FORM TO THE ABOVE ORGANIZATION.

1. REPORT DATE	**2. REPORT TYPE**	**3. DATES COVERED**	
20220920	Final	**START DATE** 20170401	**END DATE** 20220331

4. TITLE AND SUBTITLE
High Average Power Difference-Frequency Generation in the Mid-Infrared

5a. CONTRACT NUMBER	**5b. GRANT NUMBER**	**5c. PROGRAM ELEMENT NUMBER**
	FA9550-17-1-0194	61102F
5d. PROJECT NUMBER	**5e. TASK NUMBER**	**5f. WORK UNIT NUMBER**

6. AUTHOR(S)
Robbie Murray

7. PERFORMING ORGANIZATION NAME(S) AND ADDRESS(ES)
IMPERIAL COLLEGE OF SCIENCE TECHNOLOGY & MEDICINE
EXHIBITION RD
LONDON
GB

8. PERFORMING ORGANIZATION REPORT NUMBER

9. SPONSORING/MONITORING AGENCY NAME(S) AND ADDRESS(ES)	**10. SPONSOR/MONITOR'S ACRONYM(S)**	**11. SPONSOR/MONITOR'S REPORT NUMBER(S)**
EOARD UNIT 4515 APO AE 09421-4515	AFRL/AFOSR IOE	AFRL-AFOSR-UK-TR-2022-0131

12. DISTRIBUTION/AVAILABILITY STATEMENT
A Distribution Unlimited: PB Public Release

13. SUPPLEMENTARY NOTES

14. ABSTRACT
Final report describes 4 different projects undertaken during this grant. These include High average power difference frequency generation in PPLN (periodically poled lithium niobate), Near infrared Raman fibre laser systems, CSP (CdSiP2) mid-wave optical parametric amplifiers pumped by Raman fibre systems, and Novel parametric seeding architectures – cascaded four and three wave mixing.

15. SUBJECT TERMS

16. SECURITY CLASSIFICATION OF:			**17. LIMITATION OF ABSTRACT**	**18. NUMBER OF PAGES**
a. REPORT	**b. ABSTRACT**	**c. THIS PAGE**	SAR	23
U	U	U		

19a. NAME OF RESPONSIBLE PERSON	**19b. PHONE NUMBER** *(Include area code)*
ANDREW GREENWOOD	314 235 6037

EOARD Final Project Report for FA9550-17-1-0194

"High average Power Difference-Frequency Generation in the Mid-Infrared"

Principle Investigator: Dr Robbie Murray[1]
Co-investigator: Prof. J. Roy Taylor[1]
1 - Femtosecond Optics Group, Blackett Laboratory, Imperial College London, London, SW7 2BW, UK
Current programme manager: Dr Nate Lockwood
Grant period: 1st April 2017-31st March 2022 (3 x 1 year NCES granted)
Grant total: $239,976.00

Contents

Executive summary and project outputs

In this project, we have developed various novel near infrared laser systems, and used them to push the state-of-the-art in mid-infrared light generation in the 3-5 µm region, corresponding to the first atmospheric transmission window. Extensive collaboration between Imperial College London, the Airforce Research Laboratory (RX, Dayton, OH) and BAE Systems (NH, US), underpinned this work. This included two short visits (seminars), and a longer one-month research visit by Dr Murray to RX in Dayton (hosted by Dr Guha and funded by Windows on Science). For any questions on the work, please contact Dr Murray (robert.murray10@imperial.ac.uk). The following is a list of publications and conference proceedings directly resulting from the work carried out under this project agreement. Note, there is a separate section for report specific references (pg 21).

DISTRIBUTION A: Distribution approved for public release. Distribution unlimited

1) Murray, R. T., Runcorn, T. H., Guha, S. & Taylor, J. R. High average power parametric wavelength conversion at 3.31-3.48 µm in MgO:PPLN. Opt. Express 25, 343–348 (2017).

2) Runcorn, T. H., Murray, R. T. & Taylor, J. R. Microjoule Nanosecond 560 nm Source by SHG of a Combined Yb-Raman Fiber Amplifier. in Laser Congress 2017 (ASSL, LAC) ATu1A.7 (OSA, 2017).

3) Runcorn, T. H., Murray, R. T. & Taylor, J. R. High Average Power Second-Harmonic Generation of a CW Erbium Fiber MOPA. IEEE Photonics Technol. Lett. 29, 1576–1579 (2017).

4) Murray, R. T., Runcorn, T. H., Guha, S. & Taylor, J. R. Fibre MOPA pumped MIR parametric wavelength conversion (Conference Presentation) [Invited]. in Proc. SPIE 10516, Nonlinear Frequency Generation and Conversion: Materials and Devices XVII 10516–12 (2018).

5) Murray, R. T., Runcorn, T. H. & Taylor, J. R. Fibre-based Sources from the UV to Mid-Infrared. in Advanced Photonics Congress 2018 (BGPP, IPR, NP, NOMA, Sensors, Networks, SPPCom, SOF) SoTu3G.1 (OSA, 2018).

6) Chandran, A. M., Runcorn, T. H., Murray, R. T. & Taylor, J. R. 620 nm source by second harmonic generation of a phosphosilicate Raman fiber amplifier. in Conference on Lasers and Electro-Optics, Technical Digest Series (OSA Publishing Group, 2019) SM3L.4 (2019).

7) Chandran, A. M., Runcorn, T. H., Murray, R. T. & Taylor, J. R. Nanosecond pulsed 620 nm source by frequency-doubling a phosphosilicate Raman fiber amplifier. Opt. Lett. 44, 6025–6028 (2019).

8) Battle, R. A. et al. Mid-infrared parametric wavelength conversion seeded with fiber optical parametric sources. in EPJ Web of Conferences, EOSAM 2021 vol. 255 11004 (2021).

9) Murray, R. T. et al. Seeded optical parametric generation in CdSiP2 pumped by a nanosecond pulsed, MHz repetition rate Raman fiber amplifier at 1.24 µm. in Nonlinear Frequency Generation and Conversion: Materials and Devices XX (eds. Schunemann, P. G. & Schepler, K. L.) vol. 46 6 (SPIE, 2021).

10) Murray, R. T. et al. Seeded optical parametric generation in CdSiP2 pumped by a Raman fiber amplifier at 1.24 µm. Opt. Lett. 46, 2039–2042 (2021).

11) Murray, R. T. et al. CdSiP2 based mid-infrared optical parametric sources pumped with Raman fiber amplifiers. in Advanced Photonics Congress 2021 (IPR, Networks, NOMA, PVLED, SPPCom) NoW2A.1 (2021).

12) Chandran, A. M., Battle, R. A., Murray, R. T., Runcorn, T. H. & Taylor, J. R. 743 nm Source SHG of a Cascaded Phosphosilicate Raman Fiber Amplifier. Laser Congress 2021 (ASSL,LAC) AW3A.5 (2021).

13) Chandran, A. M., Battle, R. A., Murray, R. T., Runcorn, T. H. & Taylor, J. R. Watt-level 743 nm source by second-harmonic generation of a cascaded phosphosilicate Raman fiber amplifier. Opt. Express 29, 41467 (2021).

14) Battle, R. A., Chandran, A. M., Runcorn, T. H., Mussot, A., Kudlinski, A., Murray, R. T., & Taylor, J. R. (2022). Optical parametric amplification seeded by four-wave mixing in photonic crystal fibers. *Proc. SPIE 11985, Nonlinear Frequency Generation and Conversion: Materials and Devices XXI*, *1198502*, 4.

15) Murray, R. T., Anderson, J., Wei, J., Zawilski, K. T., Schunemann, P. G., & Guha, S. (2022).Wavelength tunable mid-infrared generation in non-critically cut CdSiP2 crystals by cascaded optical parametric generation with a nanosecond 1.064 µm Nd:YAG laser. *Conference on Lasers and Electro-Optics, Technical Digest Series (Optica Publishing Group, 2022)*, SM2O.2.

DISTRIBUTION A: Distribution approved for public release. Distribution unlimited

High average power difference frequency generation in PPLN

Summary

We present results of high average power mid-infrared (mid-IR) generation employing synchronized nanosecond pulsed ytterbium and erbium fiber amplifier systems using periodically poled lithium niobate. We generate greater than 6 W of mid-IR radiation tunable in wavelength between 3.31–3.48 µm, at power conversion efficiencies exceeding 75%, with near diffraction limited beam quality (M2 = 1.4). Numerical modelling is used to verify the experimental results in differing pump depletion regimes. The work in this section is summarised in various publications [1]–[6].

Experimental setup

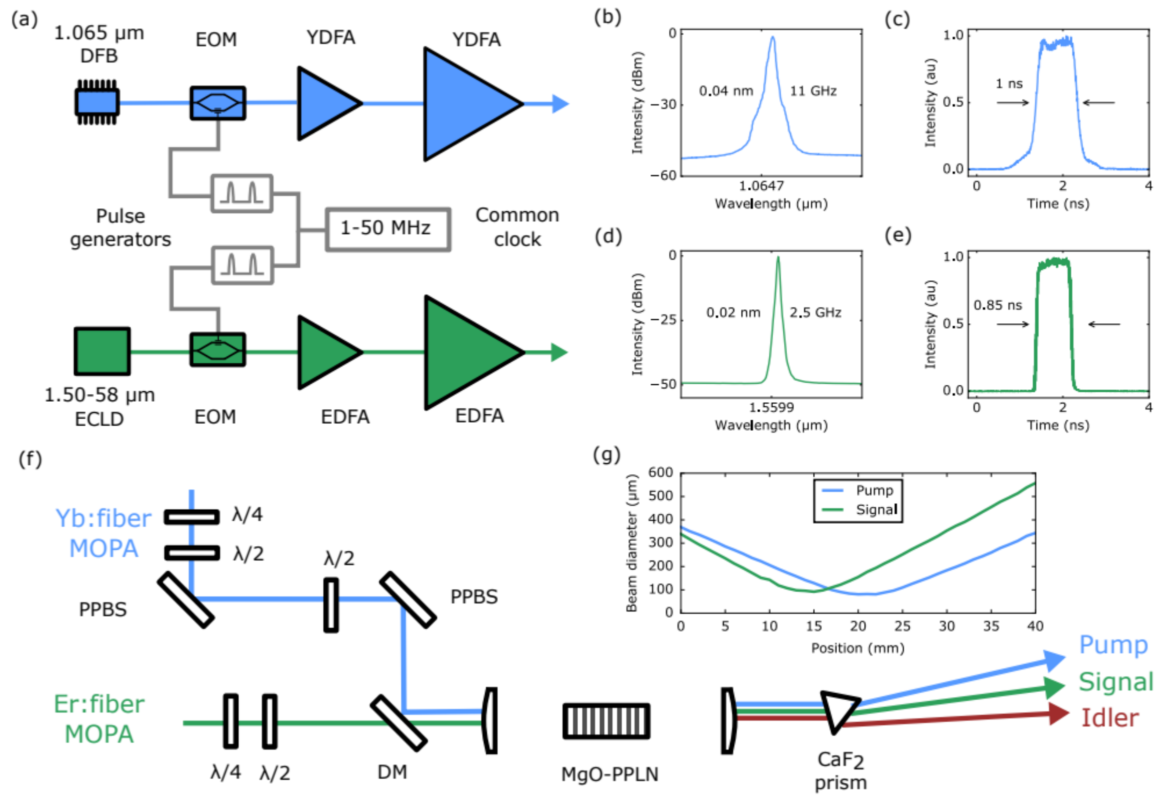

Figure 1 - Master oscillator power amplifiers (MOPAs) used for mid-infrared (mid-IR) generation, component acronyms are described in the body of the main text. (b)/(d) Example spectral and (c)/(e) temporal outputs of the Yb/Er:MOPAs. Labels show the full-width half maxima (FWHM) in wavelength, frequency and time domains respectively. MOPA output characteristics presented here represent those for optimal high average power mid-IR generation. (f) Mid-IR parametric conversion stage. The two MOPAs were combined in a 40 mm long MgO-doped periodically poled lithium niobate (MgO-PPLN) crystal. Crystal held in an insulated copper oven at temperatures from 20–230◦C. (g) Measured pump and signal beam caustics in air, at the focal position of crystal.

The experimental setup of the Yb:fiber and erbium:fiber (Er:fiber) master oscillator power amplifier (Yb/Er:fiber MOPA) systems used in this work are shown in Fig. 1. The Yb:fiber MOPA was seeded by a intensity modulated distributed feedback laser diode (DFB-LD) at 1.065 µm. The continuous wave (CW) output of the DFB-LD was modulated by a fiber coupled electro-optic modulator (EOM), producing pulses with selectable durations from 0.2–3 ns, at repetition rates of 1–50 MHz with a spectral linewidth of ∼ 40 pm [Figs. 1 (b,c)]. The Er:MOPA arm employed the same seed oscillator

DISTRIBUTION A: Distribution approved for public release. Distribution unlimited

architecture, with the DFB-LD replaced by an external-cavity laser diode (ECLD) tunable from 1.50–1.58 µm. Similar pulse duration and repetition rate parameters were accessible with the Er:MOPA [Figs. 1 (d,e)]. In both MOPAs, two fiber amplifier stages consisting of Yb or Er doped fiber amplifiers (YDFA/EDFA) were then used to amplify the seed oscillators to average powers of 27/2 W, Yb/Er:fiber MOPA respectively. In both systems the modulators were driven using synchronized electrical pulse generators. Adjustable electrical delay lines between the pulse generators enabled easy temporal overlap of the pulses. The setup was similar to that used in[7] with the exception that in this work both MOPAs used duration tunable seed oscillators, resulting in greater flexibility when optimizing the nonlinear conversion. Optimized optics were also employed, enabling ∼30% more pump power incident on the crystal than in Ref.[7]. The fiber amplifiers used in both arms were non-polarization maintaining, therefore, the output polarization state of the MOPAs tended to rotate during initial turn-on of the system. This rotation was due to temperature induced birefringence changes in the fiber. Quarter/half waveplate sets were used at the output of the MOPAs to linearize the polarization state for optimal nonlinear conversion [Fig. 1 (f)]. After approximately half an hour of operation, the MOPAs polarization state stabilized, and minimal adjustment to the output waveplates was then needed. The second half waveplate and polarizing-plate beamsplitter (PPBS) were used in the Yb:fiber MOPA arm to provide control over the average power incident on the crystal. A dichroic mirror, highly reflective for the pump and highly transmissive for the signal, was used to direct the beams towards the crystal focusing lens. An f = 75 mm lens was used to focus the incident pump and signal beams into the crystal, resulting in beam waist diameters (D4σ widths) for the pump and signal of 85 µm and 95 µm respectively. Figure 1 (g) shows the beam caustics of the pump and signal measured in air, at the focal position of the crystal. There is a ∼ 6 mm difference in focal positions for the pump and signal, attributed to chromatic aberrations of the focusing lens used, and non-ideal collimation of signal light from the Er:MOPA. With the pump pulse presented in Fig. 1 (c) [1 ns at 25 MHz], this pump spot size corresponds to a peak intensity in the crystal of ∼ 30 MW/cm2 , well below the typical damage threshold quoted for PPLN in this pump power and pulse duration range of 0.1–1 GW/cm2 [8][9].

The PPLN used throughout this work was a 40x10x1 mm crystal doped with 5% MgO (MgO-PPLN - Covesion UK). A grating period of Λ=29.98 µm was employed for all the results presented herein. The entrance and exit faces of the crystal were anti-reflection coated for the pump, signal and idler wavelengths. The crystal was held in a copper oven enclosed in an insulated PTFE housing, and the oven temperature could be adjusted from 20–230◦C with ±0.1◦C accuracy. An uncoated CaF2 plano-convex lens was then used to collimate the pump, signal and idler from the crystal, before a CaF2 prism spectrally dispersed the three beams for analysis.

Mid-IR generation

Once spatially and temporally overlapped within the PPLN crystal, efficient parametric wavelength conversion was observed between the pump and signal. Using a pump wavelength of 1.065 µm with a signal wavelength of 1.56 µm produced idler radiation at 3.35 µm [Fig. 2 (b)]. The GHz linewidth MOPAs used as the pump and signal [Fig. 1 (b/d)] transfer their narrow spectral linewidths to the mid-IR, resulting in the generation of idler radiation with linewidths on the order of Δ f ∼ 5 GHz [Fig. 2 (b)]. By tuning the temperature of the oven (133–210◦C) and the corresponding signal wavelength of the Er:MOPA (1.535–1.570 µm), it was possible to tune the idler over the range 3.31–3.48 µm. Example spectra from a truncated section of this tuning range are presented in Fig. 2 (a). Spectra beyond 3.4 µm were not measured in this work, due to limitations of the measurement range of the optical spectrum analyzer used (Yokogawa AQ6376). However, the existence of the longer wavelength idler radiation (> 3.4 µm) was confirmed through the measurement of the amplified signal wavelength and the signal and idler powers, and was also demonstrated in our earlier work [7]. An example optimized

DISTRIBUTION A: Distribution approved for public release. Distribution unlimited

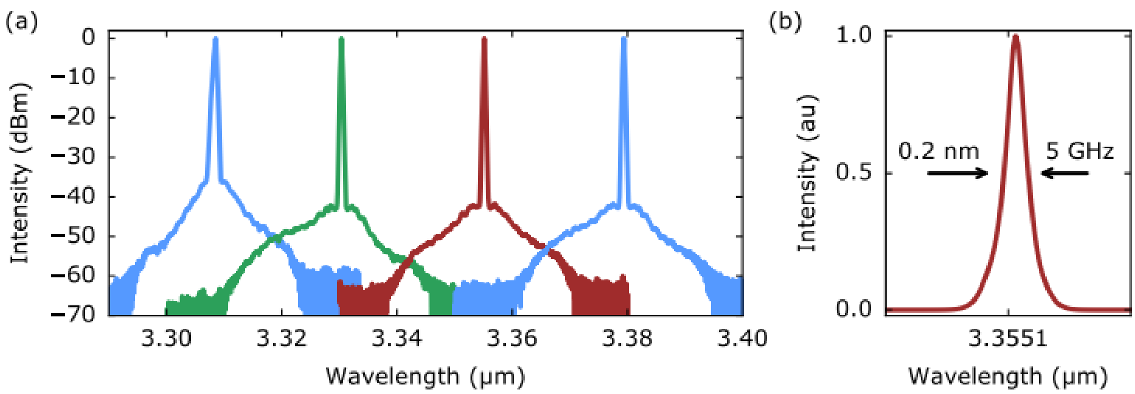

Figure 2 - Idler spectral tuning - note that the full tuning range is not shown due to the optical spectrum analyzers measurement range. (b) Example idler spectrum plotted on linear scale, with full-width half maximum spectral widths (wavelength and frequency) indicated, resolution limit of OSA was 0.1 nm.

power curve for the source is shown in Fig. 3 (a), with the corresponding pump conversion shown in Fig. 3 (b). We define the pump conversion as being the proportion of pump photons converted to the amplified signal, generated idler or both. In contrast to our previous work where we observed strong back-conversion of the signal/idler to the pump [7], the pump conversion only begins to roll off at the highest available pump power. This was readily achieved by adjusting the peak pump intensity in the crystal using two methods: coarse adjustment using different crystal focusing lenses, and finer adjustment through pump/signal duration and/or repetition rate tuning. At the maximum available pump power of 25.5 W at the crystal face, we produced 12.7 W of amplified signal and 6.2 W of generated idler, corresponding to a maximum total pump conversion of 75%. An input signal power of 1.6 W (in the crystal) was used throughout, corresponding to a maximum signal gain of 9.5 dB. The generated powers were also very stable, with the idler power exhibiting a root-mean-square (RMS) power deviation of < 0.3% over a 3 hour test period. The presented average powers account for losses from the uncoated CaF2 optics after the crystal, and therefore, represent powers at the exit face of the crystal directly. The combination of high average powers, tunable from 3.31–3.48 μm with GHz spectral linewidths, mean that this source could be suitable for mid-IR spectroscopic applications requiring high spectral power densities.

The results presented in Fig. 3 are typical of the source performance across its spectral tuning range, with greater than 6.0 W of mid-IR light produced from 3.31–3.48 μm. Further wavelength tuning was not possible due to restrictions on the Er:MOPA gain bandwidth. These results represent, to the best of our knowledge, the highest average powers generated through single-pass parametric wavelength conversion in PPLN utilizing fiber pump systems. Higher average powers have been demonstrated in [10], but a more complex dual stage OPO/OPA scheme was employed for the parametric conversion. A large footprint Nd:YAG slab MOPA pump source was also used, resulting in relatively low brightness idler radiation with M2 values of ~ 4.

DISTRIBUTION A: Distribution approved for public release. Distribution unlimited

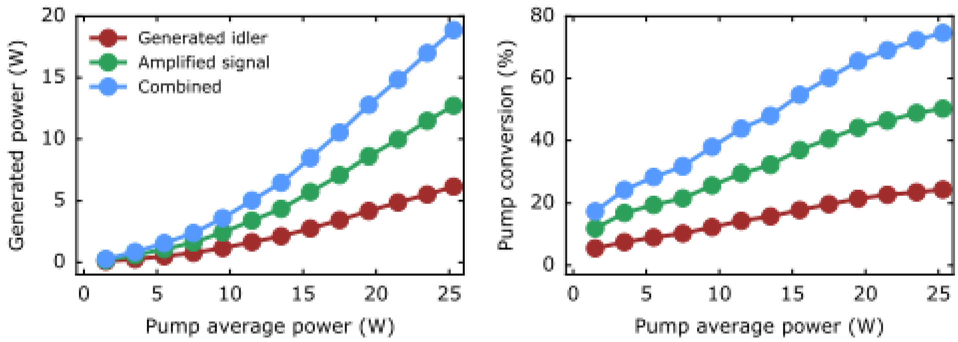

Figure 3 - (a) Example amplified signal (green), generated idler (red) and combined (blue) powers produced during parametric conversion. (b) Typical pump conversion to the signal, idler and combined wavelengths.

In contrast to their bulk laser counterparts, fiber lasers are compact, efficient and robust, and have the additional benefit of possessing inherent excellent beam quality. The pump and signal fiber:MOPAs used in this work both had M2 < 1.1, and Fig. 4 reveals that the beam quality of the mid-IR radiation at full power was also excellent (M2 = 1.4). The slight degradation in beam quality in the conversion process can be attributed to the Gaussian beam profiles of the pump and signal MOPAs. Nonlinear conversion across the profiles of the pump/signal/idler due to the transverse intensity profiles will lead to some low-level back-conversion effects in the presence of high pump depletion effects. Possible beam quality improvement may be possible; it has been shown that gain-guiding and back-conversion effects can be counter-balanced by adjusting the focusing conditions in the crystal [11]. Beam quality degradation could also be alleviated through the use of flat-top beam profiles rather than Gaussian, leading to uniform nonlinear conversion across the transverse axes of the beams.

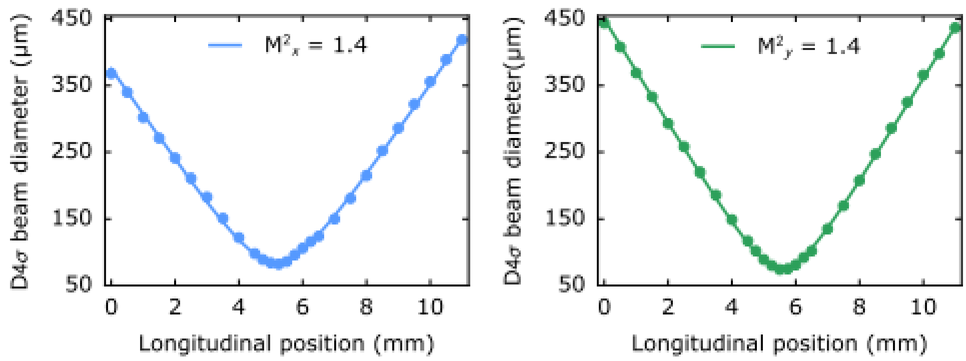

Figure 4 - Measured beam diameter (D4σ widths) of the idler in the horizontal and vertical beam axis through the focus of a lens, with a Gaussian fit to the beam caustic. Taken at full power and measured using a pyroelectric scanning slit beam profiler.

Figure 5 shows the measured traces of the pump and signal pulses as a function of increasing pump conversion. The pulse amplitudes are normalized for easier comparison. The idler pulses could not be measured directly due to a lack of diagnostics in the mid-IR, but can be inferred from the amplified signal traces. The pump pulses underwent increasing depletion with increasing conversion, with the center of the pulse being almost completely depleted at the highest conversion level (75%). The

DISTRIBUTION A: Distribution approved for public release. Distribution unlimited

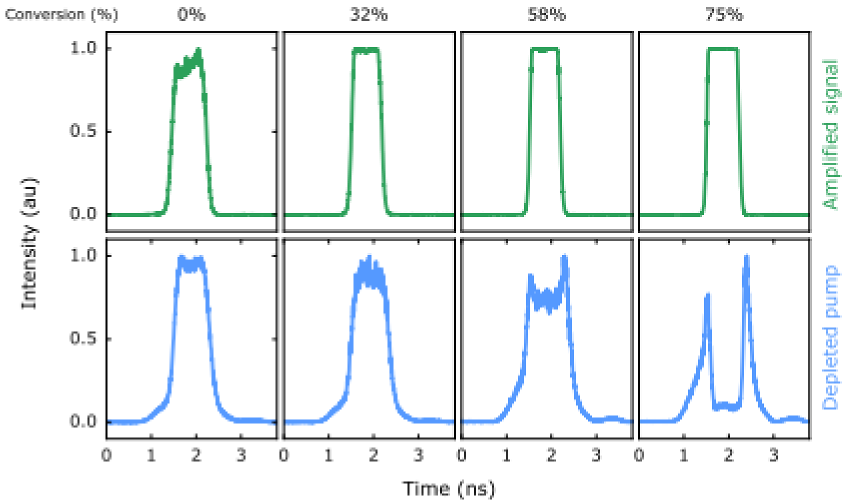

Figure 5 - Sampling optical oscilloscope traces of signal and pump for increasing levels of pump conversion, from 0% to 75%, after undergoing parametric conversion in PPLN. Signal pulses shown on top row in green, with corresponding pump pulses on the bottom row in blue. All pulse amplitudes are normalized.

corresponding signal pulse duration decreased slightly with increasing conversion, from 850 ps initially to 730 ps at 75% pump conversion. A slight shortening was expected due to the finite rise and fall time of the pump/signal pulses. The electrical pulsers used to drive the respective EOMs in each MOPA arm were also slightly different, thus, the shape of the pump and signal pulses did not match exactly. Improved conversion efficiency could be expected with better pump and signal pulse overlap, in particular, the use of more rectangular pulses with faster rising and falling edges. There was also no obvious sign of back-conversion in the temporal domain, in contrast to our previous work [7]. The use of duration tunable pump and signal MOPAs allowed easy optimization of the nonlinear conversion at any average power level, avoiding unwanted excessive back-conversion. This feature is essential for further power scaling of mid-IR average power levels using this configuration.

Near infrared Raman fibre laser systems

Summary

In this work, we demonstrated a source emitting at 620 nm based on the frequency doubling of Raman fibre amplifier at 1.24 µm [12], [13]. The generation of red light is not related to this project (separate project aimed at biophotonics imaging applications) but the development of the Raman fiber amplifier is crucial for the generation of light in the difficult to reach region of 4-5 µm, using non-oxide based crystals, such as cadmium silicon phosphide ($CdSiP_2$).

The Raman fiber amplifier at 1.24 µm has excellent properties for pumping optical parametric amplifiers (OPAs) to generate light in the mid-infrared. These include near-diffraction limited beam quality (M^2<1.1), average powers of up to 10 W, peak powers of 2 kW, and tunable pulse duration (50 ps-2 ns) and repetition rates (1-100 MHZ). The system schematic is shown in Figure 7, with some example system results shown in Fig 6.

DISTRIBUTION A: Distribution approved for public release. Distribution unlimited

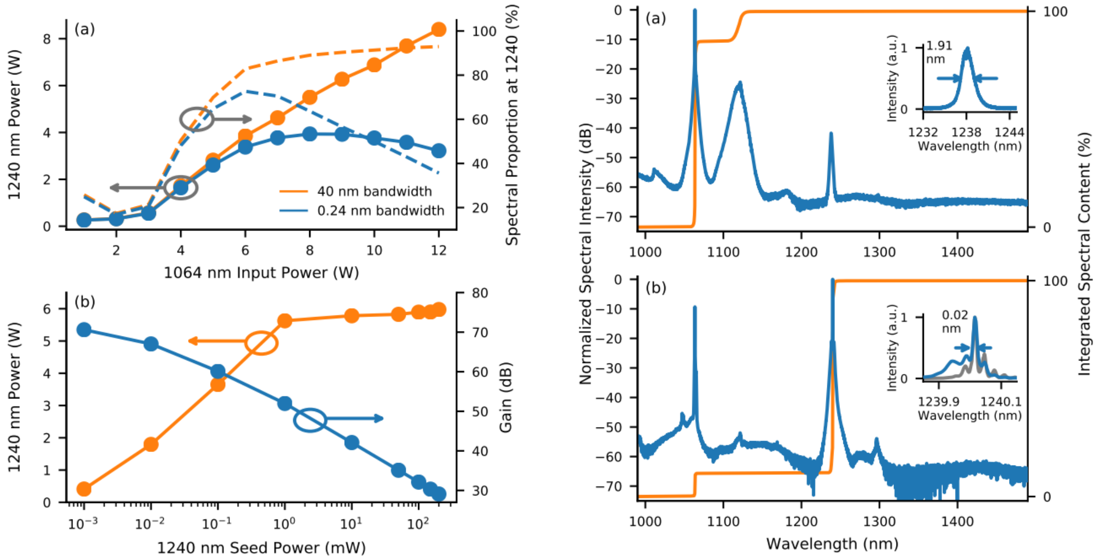

Figure 6 - (a) Calculated phosphosilicate Raman fiber amplifier output power (points) and percentage spectral content (dashed lines) as a function of input 1064 nm power for a 40 nm (orange) and 0.24 nm (blue) integration bandwidth at 1240 nm. (b) Generated 1240 nm power (orange) and phosphosilicate Raman fiber amplifier gain (blue) as a function of seed power, for an Yb:fiber MOPA power of 8W. Spectra of the phosphosilicate Raman fiber amplifier output for a 1064nm input power of8W where (a) no seed light is present and (b) 200 mW of seed power are coupled into the phosphosilicate fiber. The orange lines show the integrated spectral content as a function of wavelength. Insets show optical spectrum of the generated 1240 nm light (blue) and 1240nm seed diode (gray) on a linear scale.

This novel approach employs heavily doped phosphosilicate fibres as the Raman gain medium. Such fibres exhibit a substantially larger Raman shift than conventional optical fibres (40 THz vs 13 THz). Yb fibre amplifiers emitting around 1 µm can therefore be shifted directly to the 1.2X µm, ideal for pumping CSP based OPAs phasematched with non-critical phasematching (NCPM). Such systems can be fully fibre integrated, leading to robust, compact and field deployable pump systems for mid-infrared OPAs. By selecting different starting Yb:fibre pump wavelengths and different Raman conversion media, it is possible to create high power fibre based sources in the 1.1-1.5 µm ideal for NCPM CSP OPAs.

DISTRIBUTION A: Distribution approved for public release. Distribution unlimited

Experimental setup and results

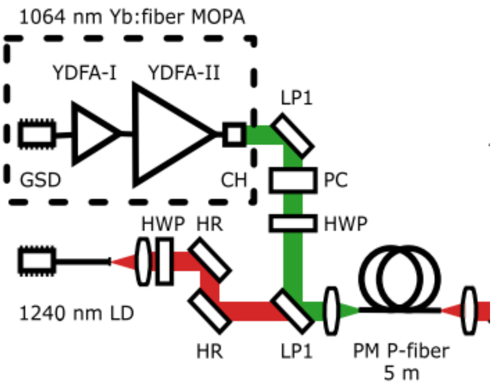

Figure 7 - 1240 nm phosphosilicate Raman fiber - GSD, gain-switched laser diode; YDFA-I, Yb-doped fiber pre- amplifier; YDFA-II, Yb-doped fiber power amplifier; CH, collimator head; LD, laser diode; P-fiber, phosphosilicate fiber; HWP, half-wave plate; PC, power control, formed of half-wave plate and polarizing beam splitter cube; HR, highly reflective mirror at 1240 nm; LP1, longpass filter (cut-on 1150 nm).

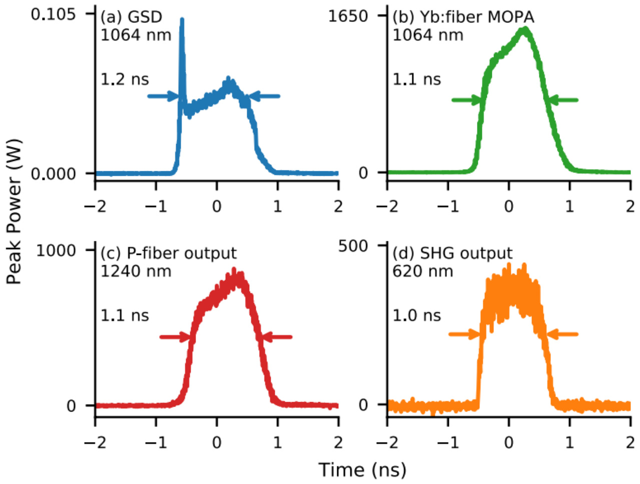

Figure 8 - Temporal profiles of the output pulses of the (a) 1064 nm gain-switched laser diode (GSD), (b) Yb:fiber MOPA, (c) phosphosilicate fiber (P-fiber) amplifier, and (d) 620 nm SHG output from the PPLT crystal. The full-width-half-maximum (FWHM) pulse duration is indicated in each case.

A pulsed Yb:fiber MOPA system operating at 1064 nm was converted to 1240 nm in a phosphosilicate Raman fiber amplifier, seeded by a narrow-linewidth CW laser diode at 1240 nm. The generated 1240 nm light adopts the temporal properties of the Yb:fiber MOPA system, as the Raman gain is available only in the window of the 1064 nm pulses [14]. Using a 1240 nm seed diode operating CW avoids the need for any synchronization electronics with the Yb:fiber MOPA pulses. The 1240 nm light was subsequently frequency-doubled in a periodically poled stoichiometric lithium tantalate (PPLT) crystal. The source had near-diffraction-limited beam quality (M2 ≤ 1.16), subnanometer spectral linewidth (≤100 pm), and ideal parameters for biophotonics imaging applications such as STED microscopy and OR-PAM. This is, to the best of our knowledge, the first demonstration of a frequency-doubled phosphosilicate Raman fiber amplifier.

DISTRIBUTION A: Distribution approved for public release. Distribution unlimited

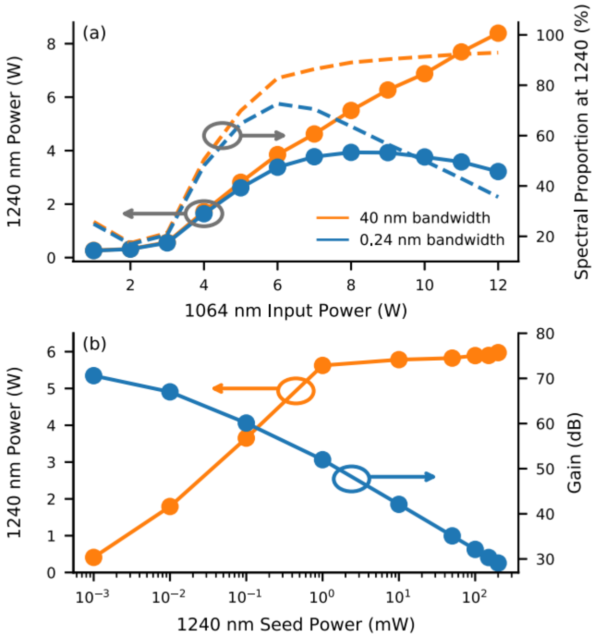

Figure 9 - (a) Calculated phosphosilicate Raman fiber amplifier output power (points) and percentage spectral content (dashed lines) as a function of input 1064 nm power for a 40 nm (orange) and 0.24 nm (blue) integration bandwidth at 1240 nm. (b) Generated 1240 nm power (orange) and phosphosilicate Raman fiber amplifier gain (blue) as a function of seed power, for an Yb:fiber MOPA power of 8 W

A 1064 nm gain-switched laser diode (QDLaser) provided pulses of 1.2 ns duration at a repetition rate of 5 MHz, with a pulse energy of 64 pJ. These pulses were amplified to a pulse energy of 900 pJ in a polarization-maintaining (PM) Yb:fiber pre-amplifier, and then to 1.5 µJ in a PM Yb:fiber poweramplifier (IPG Photonics), Fig. 7 . The temporal profile of the laser diode output pulses and power amplifier pulses can be seen in Figs. 8 (a) and 8(b), respectively. The relaxation oscillation at the leading edge of the diode pulse, 50 ps in duration, is characteristic of the pulse dynamics in gain-switched laser diodes [15].

A 5 m length of PM phosphosilicate fiber (FORC P-SM-5- PM, PM P-fiber) was used as the Raman fiber amplifier gain medium. The length of phosphosilicate fiber used, in conjunction with the chosen 1064 nm input peak power, must be carefully chosen to minimize deleterious nonlinear effects and the onset of other Raman Stokes shifts while maintaining a high level of conversion to 1240 nm. These Stokes lines include those at 1120 nm and 1310 nm due to the 13 THz Raman shift, and at 1480 nm, due to the 40 THz Raman shift.

A fiber Bragg grating stabilized laser diode operating at 1240 nm (Innolume) was used to provide a CW, linearly polarized seed signal to the Raman amplifier. The diode provided up to 300 mW of power at 1240 nm, with a 3 dB spectral linewidth of 20 pm. A maximum of 200 mW of 1240 nm light was coupled into the phosphosilicate fiber. The 1064 nm pump and 1240 nm seed beams were combined using a pair of longpass filters with a cut-on at 1150 nm (Thorlabs DMLP1150). The use of PM components throughout the system ensured that both the 1064 nm Yb:fiber amplifier output pulses and 1240 nm seed light were linearly polarized and coupled onto one of the principal axes of the phosphosilicate Raman fiber, to maximize the Raman gain.

DISTRIBUTION A: Distribution approved for public release. Distribution unlimited

Figure 9(a) shows that the average power at 1240 nm generated within a bandwidth of 40 nm, sufficient to incorporate the entire spectral feature at 1240 nm, increases monotonically with 1064 nm input power (orange points). However, the average 1240 nm power generated within a smaller bandwidth of 0.24 nm (the spectral acceptance bandwidth of the PPLT crystal, discussed later) begins to roll-off at 1064 nm input powers of greater than 8 W (blue points). The 3 dB spectral linewidth of the amplified 1240 nm signal was 20 pm for all amplifier output powers up to 12 W. This was the same as the 3 dB linewidth of the 1240 nm seed diode, showing that there was no spectral broadening of the linewidth due to nonlinear effects such as self-phase modulation. The roll-off in power was instead due to the growth of a pedestal around the 1240 nm signal. Any power outside the 0.24 nm spectral acceptance bandwidth of the PPLT crystal will decrease the SHG conversion efficiency. Thus, the Raman amplifier was operated at a power of 7.5 W for the frequency doubling.

Figure 9(b) shows the generated average power at 1240 nm (orange points) and the corresponding amplifier gain (blue points) as a function of 1240 nm seed power for a 1064 nm input power of 8 W. Above a seed power of 1 mW, there was a sharp roll-off in the generated 1240 nm power, and the amplifier gain strongly saturated with increasing seed power. The amplifier gain was calculated using the effective seed power, rather than the total 1240 nm seed power coupled into the phosphosilicate fiber. This effective seed power was the total 1240 nm seed power divided by the duty cycle of the Yb:fiber MOPA system, since the Raman gain is negligible outside the pump pulses.

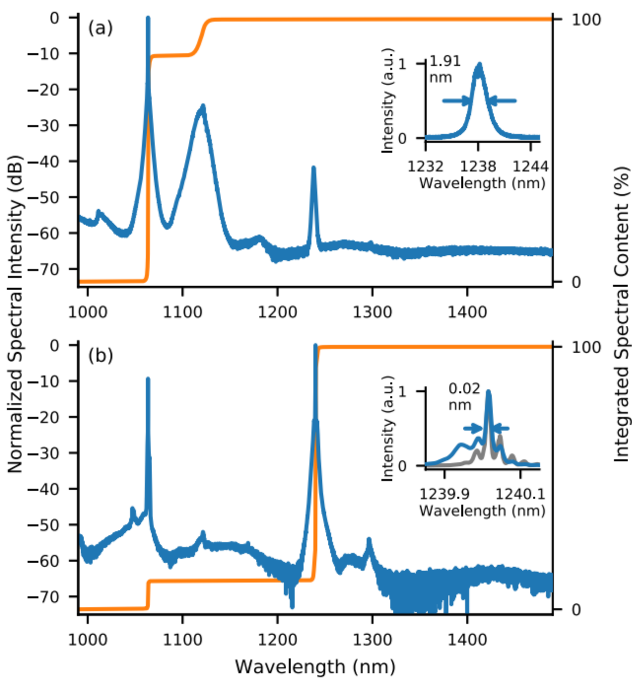

Figure 10 - Spectra of the phosphosilicate Raman fiber amplifier output for a 1064 nm input power of 8 W where (a) no seed light is present and (b) 200 mW of seed power are coupled into the phosphosilicate fiber. The orange lines show the integrated spectral content as a function of wavelength. Insets show optical spectrum of the generated 1240 nm light (blue) and 1240 nm seed diode (gray) on a linear scale.

DISTRIBUTION A: Distribution approved for public release. Distribution unlimited

Figure 10(a) shows the optical spectrum of the phosphosilicate Raman fiber amplifier output at a 1064 nm input power of 8 W in the case where no seed light is present, as well as the integrated spectral content as a function of wavelength. In the unseeded case, only 0.07% of the output spectral content was contained within a 40 nm bandwidth centered at 1240 nm. The majority of the spectral content instead comprised the residual 1064 nm input power and light at the first 13 THz Raman Stokes shift at 1120 nm. Moreover, the linewidth of the generated 1240 nm was broad, with a 3 dB spectral bandwidth of 1.91 nm. In contrast, Fig. 10(b)shows the optical spectrum of the phosphosilicate Raman fiber amplifier output for 8 W of 1064 nm input power and 200 mW of coupled 1240 nm seed power. In this case, 89% of the light was contained within a 40 nm bandwidth centered at 1240 nm.

The Raman fiber amplifier was highly efficient; the conversion efficiency from 1064 nm input power to 1240 nm output power was 66% at a 1064 nm input power of 8 W. Accounting for coupling losses, the internal conversion efficiency of 1064 nm to 1240 nm in the Raman fiber amplifier was 79%, close to the maximum quantum defect limited conversion efficiency of 85%. The temporal profile of the generated 1240 nm pulses can be seen in Fig. 8(c). The pulses have a full-width-half-maximum (FWHM) duration of 1.1 ns and follow the temporal profile of the 1064 nm pump pulses [Fig. 8(b)]. The phosphosilicatefiber used has a cutoff wavelength of <1060 nm and is therefore single mode for both the pump and signal wavelengths. The beam quality of the amplified 1240 nm signal was measured to be M2 = 1.01 using a pyroelectric scanning slit beam profiler.

CSP mid-wave optical parametric amplifiers pumped by Raman fibre systems

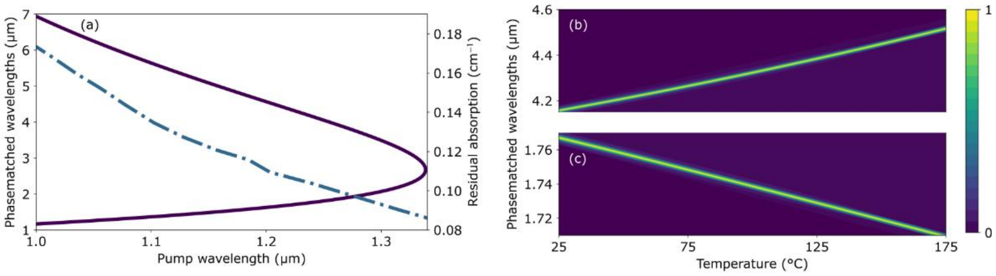

Figure 11 - (a) Phasematched signal and idler wavelengths for non-critical 90° type-I (oo-e) in CSP, purple solid line. Residual absorption of CSP as a function of pump wavelength, dashed-dotted blue line. (b) Phasematched idler and signal (c) wavelengths against crystal temperature, colorbar indicates the theoretical conversion efficiency.

Summary

In this work, we demonstrated the first application of a Raman fiber amplifier system for pumping a CSP OPA emitting light in the hard-to-reach 4-5 μm region [16]–[19]. The CSP was obtained from BAE Systems through the AFRL/EOARD, partially funded by a separate project - Functional Materials Division of the Materials and Manufacturing Directorate, Air Force Research Laboratory (AFRL/RXA) (FA8650-16-F-5418). The non-critical phasematching diagrams for pumping CSP in the 1-1.4 μm region are shown in Figure 11.

The Raman fibre amplifier (described fully in [12]) was used to pump a CSP optical parametric generator, seeded with a fibre supercontinuum source, as shown in Figure 12. Simple temperature tuning of the crystal leads to a broadly tunable output in the 4.2-4.6 μm as shown in Figure 16.

This is the first demonstration of MHz repetition rate pumping of CSP in the 1.2 μm region, and the first demonstration of such widely tunable idler radiation with this pump wavelength. The pairing of

DISTRIBUTION A: Distribution approved for public release. Distribution unlimited

CSP and NIR Raman amplifiers in the 1.1–1.3 µm region represents an exciting new architecture with the potential to create high power, widely tunable radiation in the hard to access, but technologically important, 4–5 µm region of the MIR. Raman fiber sources are available at arbitrary wavelengths throughout the NIR, and CSP can be used to NCPM pump light in this region.

However, more work is needed to fully understand the potential of this architecture, in particular around the limitations of the linear and nonlinear absorption of CSP at Raman pump wavelengths throughout the NIR. We have found that operating CSP at elevated temperatures for prolonged periods may increase the susceptibility of the material to laser induced damage. This finding is particularly interesting as it places a potential upper limit on the wavelength tunability possible through temperature-tuned NCPM CSP based devices, which is one of the most attractive prospects of the NCPM architecture. Ongoing work is aimed at employing different Raman pump amplifier systems throughout the 1.1–1.3 µm region to demonstrate the full capability of this architecture. We are working to demonstrate further power scaling of the generated MIR light as proposed, and quantify further the different effects contributing to the degradation in the idler beam quality.

Experimental setup

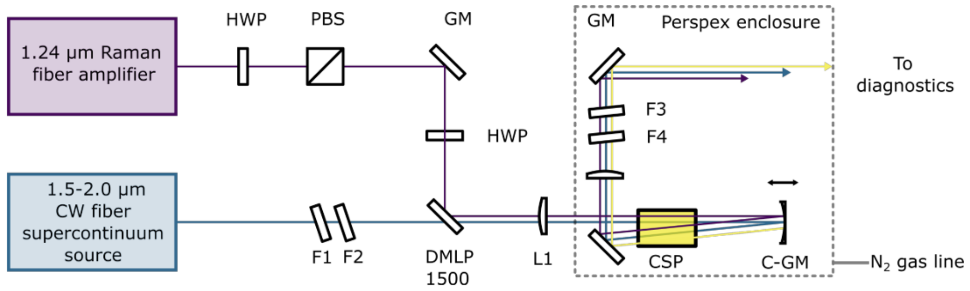

Figure 12 - Experimental setup for seeded optical parametric in CSP. The 1.24 µm Raman fiber amplifier acts as the pump with a continuous wave fiber supercontinuum source providing the seed signal, pumping the CSP crystal in a double pass configuration to generate idler radiation in the 4.2–4.6 µm band.

In this experiment, the 1.24 µm pulsed Raman fiber amplifier acts as the pump, and is combined with a continuous-wave (CW) fiber SC signal in the CSP crystal, Fig. 12. The CW-SC signal seeds the OPG process driven by the pulsed Raman fiber amplifier. The 1.24 µm pump source is based on a phosphosilicate Raman fiber amplifier architecture similar to our previous work [12]. It is tunable in repetition rate (1–20 MHz) and pulse duration (0.05–2 ns). In this work, pulses with a duration of 1 ns and a repetition rate of 3 MHz are employed, with average powers of up to 3W and a maximum pump pulse energy of 1µJ. The corresponding pump optical spectrum and temporal profile at full power can be seen in Figs. 13(a) and 13(c). The pump power in the crystal is controlled with a polarizing beam splitter (PBS) and half-wave plate (HWP). A second HWP is used to align the pump polarization to the CSP crystal axis for type-I (oo-e) NCPM.

The CW-SC signal beam in the system serves a dual purpose—it acts as a broadband seed for the OPG enabling easy wavelength tuning of the MIR idler and also crucially lowers the threshold pump intensity to initiate strong conversion through seeded OPG. A double-pass of the crystal also lowers the threshold further. This is important due to the susceptibility of CSP to laser induced damage, with reported damage threshold values for a 1.06 µm pump of approximately 44 MW/cm2 or 0.35 J/cm2

DISTRIBUTION A: Distribution approved for public release. Distribution unlimited

[20]. Shifting the wavelength away from the crystal bandgap and transmission edge, as we demonstrate in this work, is expected to result in an increase in these values.

Employing a CW-SC also avoids the need for temporal synchronization of the pump and signal light. The in-house developed CW-SC source emits radiation from approximately 1.5–2.1 µm, and two interference filters (F1/2) are used to select light at the phase-matched signal wavelength. After filtering, 200 mW of power spanning 25 nm (full width at half-maximum) at 1.72 µm is available as a seed. The central wavelength of the SC signal can be tuned by adjusting the angles of the interference filters (F1/2). An example spectrum is shown in Fig. 13(b). The modulations present in the spectrum are due to the transmission properties of the interference filters. It should be noted that this signal light is effectively unpolarized, and so only half of the signal power will contribute to the seeding process. Due to the CW nature of the SC seed, the effective signal seed power which experiences amplification, is reduced by the pump duty cycle (300), to approximately 0.3 mW.

The pump and signal beams are then combined using a longpass dichroic mirror (DMLP1500). The beams are focused into the crystal using an anti-reflection (AR) coated plano–convex lens (L1, f = 62.5 mm), resulting in a focused circular pump beam waist diameter of ≈60 µm. This corresponds to

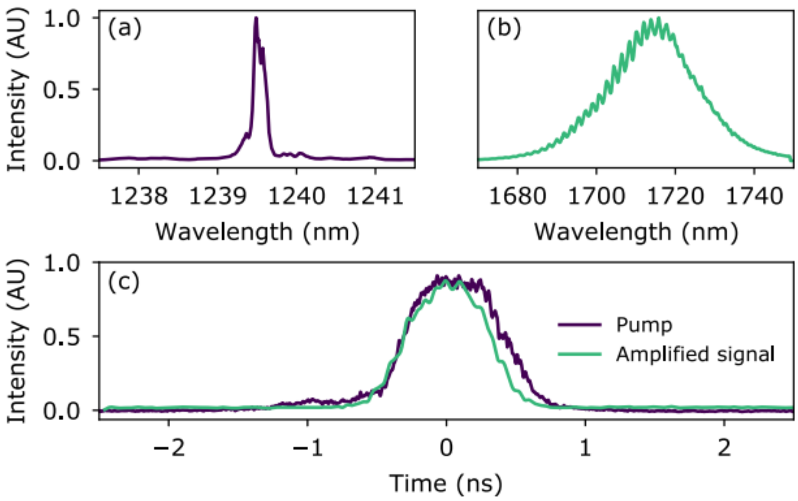

Figure 13 - a) Optical spectrum of Raman fiber amplifier pump pulses, and (b) continuous-wave filtered fiber supercontinuum signal seed. (c) Temporal profiles of pump and amplified signal pulses.

DISTRIBUTION A: Distribution approved for public release. Distribution unlimited

a maximum pump intensity of 54 MW/cm2 and a pulse fluence of 0.06 J/cm2 , slightly above the 1.06 µm literature value for the damage threshold of CSP of 44 MW/cm2 [20]. The beam waist is measured in air using a pyroelectric scanning slit profiler, which also allows easy overlap of the pump and signal beams. The CSP crystal employed is 13 mm long with an aperture of 3 × 6 mm2 . The crystal is cut at 90◦ for type-I (oo-e) NCPM, and pumping at 1.24 µm generates light around 1.76 µm and 4.2 µm, Fig 11. The crystal is held in a copper oven in PTFE housing, temperature adjustable from 25–250◦C. The crystal faces are AR coated (LaserOptik GmbH) for the pump, signal, and idler wavelengths, with single-pass transmission values of Tp = 0.93 (measured), and Ts = 0.91 and Ti = 0.95 (manufacturer quoted), respectively.

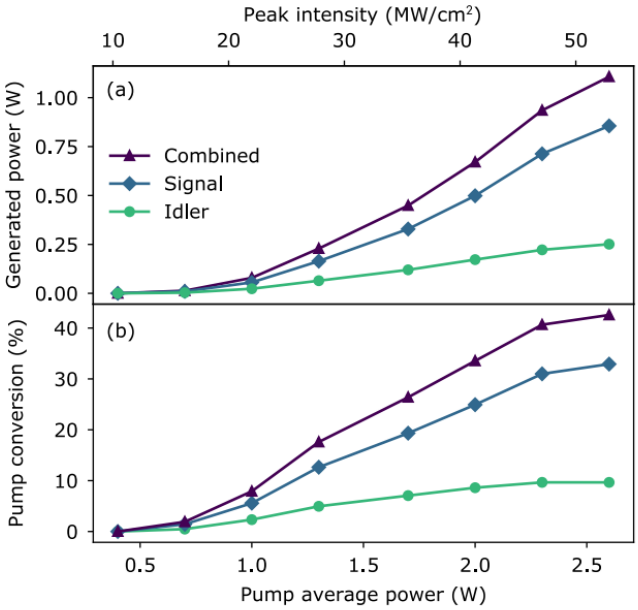

Figure 14 - (a) Signal, idler, and combined (signal plus idler) average powers against pump average power (bottom axis)/pump peak intensity in the crystal (top axis). (b) The corresponding pump conversion into the signal, idler, and combined (signal plus idler). λs = 1.76 µm and λi = 4.20 µm.

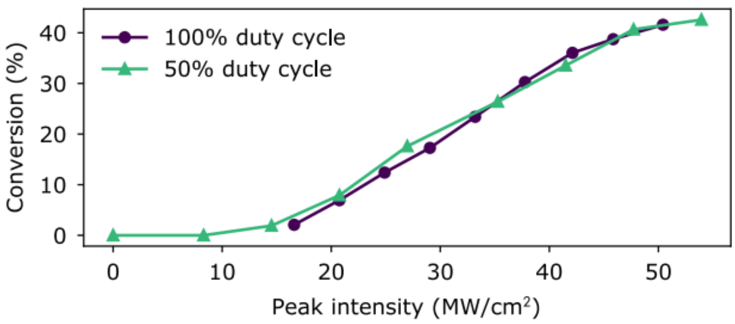

Figure 15 - Total pump conversion (combined signal plus idler) at different duty cycles. λs = 1.76 µm and λi = 4.20 µm.

After the first pass through the CSP, a curved gold mirror (C-GM, f = 50 mm) is used to reflect the residual pump, amplified signal, and newly generated idler light back through the crystal. The mirror is positioned at a distance of 2f from the CSP crystal to refocus the returning beam to match the outgoing waist size. The double-pass arrangement is essential for the seeded OPG to reach threshold at a low enough pump power for efficient conversion—in the single-pass case, threshold is only just reached at the maximum available pump power. The returning beam is offset slightly from the

DISTRIBUTION A: Distribution approved for public release. Distribution unlimited

outgoing beam waist and a gold D-shaped mirror (D-GM) is used to pick the beam off after the second pass. A CaF2 lens (L2, f = 50 mm) re-collimates the light from the double-pass arrangement. Interference filters are used after the collimating lens to separate the pump, signal, and idler radiation (F3/4, Thorlabs FB1750-500 and FB4250-500). After ensuring optimal overlap of the pump and signal beams in the crystal and adjustment of the longitudinal position of the curved gold mirror, seeded OPG is observed.

The signal and idler powers generated from the CSP as a function of pump power are shown in Fig. 14. The pump power is the power at the input face of the crystal, and the signal and idler powers are those at the exit face of the crystal and are corrected for losses through the filtering optics. The pump power is controlled with the PBS and HWP after the Raman fiber amplifier, ensuring the spectral properties of the pump remain the same throughout the experiment. Up to 250 mW of power is generated around 4.20 µm, corresponding to a pump to idler conversion of 10%. The total pump conversion, signal plus idler power, exceeds 42%. One route to increasing this conversion is to increase the peak intensity in the crystal through tighter focusing, but this is not feasible as we are already operating above the quoted damage threshold of CSP [20].

The measured idler power is very stable, fluctuating by less than 2% (peak-to-peak) over a 1 h measurement interval. However, strong roll-off in the conversion efficiency is observed at the highest pump powers. To investigate this further, a 50% duty cycle chopper wheel (CH) is used to reduce the average power and thermal load in the CSP, while maintaining the same instantaneous peak intensity. However, as seen in Fig. 15, this average power reduction is found to make no significant difference to the conversion, indicating that the roll-off in efficiency is due to either nonlinear absorption of the pump, signal, or idler light, or saturation of the parametric conversion.

As the roll-off in conversion efficiency is not linked to excessive average power, and hence thermal load, we propose further power scaling could be possible. Increasing the pulse duration and corresponding pulse energy while maintaining the same irradiance in the crystal, it could be possible to maintain the same conversion efficiencies at higher average power levels and pulse energies. Thermal lensing and dephasing, however, have been shown to be issues in high-average power CSP

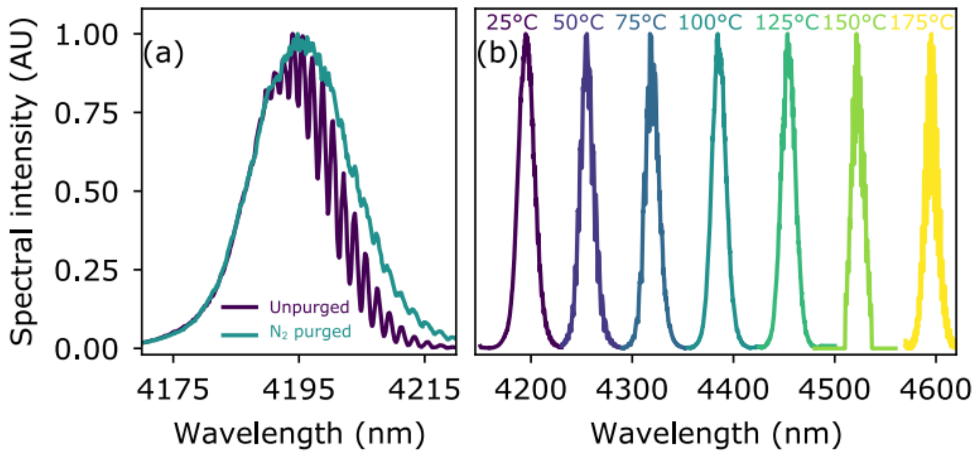

Figure 16 - (a) Example MIR idler spectrum at 25◦C, in both the unpurged and N2 purged case. (b) Wide idler wavelength tuning possible through temperature tuning the CSP crystal.

OPGs [21]. Owing to the differences in focused beam sizes, crystal absorption coefficients and interaction wavelengths in our work compared to those in [21], direct thermal effect threshold comparisons are not possible. We note that our system is currently operating well below the fluence

DISTRIBUTION A: Distribution approved for public release. Distribution unlimited

damage threshold for CSP— 0.06 J/cm2 in this work compared to the damage threshold of 0.35 J/cm2 in [20]—so an ∼5x increase in fluence should be possible before the onset of fluence related damage. This scaling may be limited by thermal issues at some threshold, but further experiments are needed to determine this point.

An example spectrum of the MIR idler output is shown in Fig. 16(a), centered around 4.2 µm. Due to atmospheric carbon dioxide, absorption lines are clearly evident in the idler spectrum. Enclosing the source in a perspex enclosure and purging with pure nitrogen gas leads to an almost complete elimination of the modulations in the spectrum. By temperature tuning the crystal oven in the range 25–175◦C, the idler wavelength can be tuned over the range 4.19–4.60µm, shown in Fig. 16(b).

Increasing the temperature beyond 175◦C results in bulk crystal damage, observed as a sudden drop in output power from the crystal and beam quality degradation. We propose that this damage occurs due to the decrease in bandgap energy associated with an increase in temperature, leading to greater near-bandgap absorption, crystal heating, and subsequent damage. We estimate 1Eg ≈ −0.06 eV for 1T = 150◦C, using data in Refs in [22]. Increased absorption from free carriers may also play a role in the increased damage susceptibility at elevated temperatures.

The absorption of CSP also decreases at lower temperatures [23]. It is also observed that the pump beam changes shape after passing through the crystal at higher pump powers, observed on a IR viewing card (Thorlabs VCR2). Crystal temperature adjustment at a constant pump power also results in changes in beam shape. We attribute this effect to the absorption change in CSP with varying temperature. Further work is required to quantify this effect fully.

The idler beam quality at ≈ 200 mW of MIR output power, is shown in Fig. 17. An f = 150 mm lens focuses the beam down to a waist, and a pyroelectric scanning slit beam profiler maps the 4σ beam diameters in the horizontal and vertical transverse planes. A Gaussian fit is used to extract the M2 values of the beam. Given the 1.24 µm pump beam is diffraction limited (M2 x ≈ M2 y ≈ 1), the idler beam quality is degraded to M2 x = 1.97 and M2 y = 1.71. Due to the issues around the residual absorption of CSP and associated laser induced damage and beam shape fluctuations we have

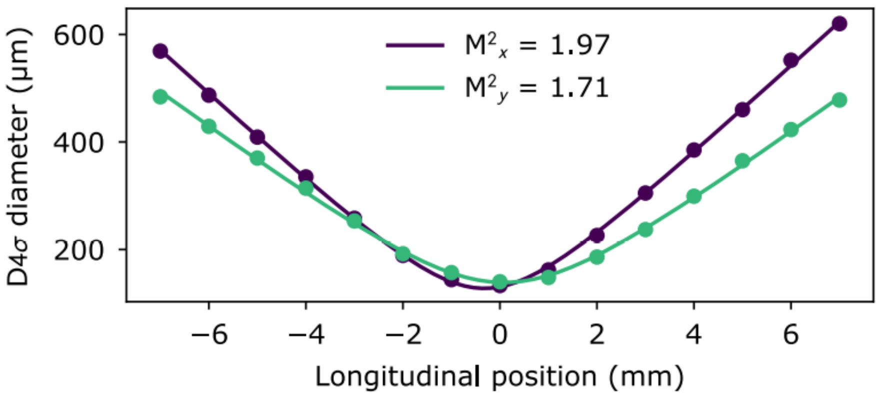

Figure 17 - Measured beam diameter (D4σ widths) of the idler in the horizontal (x) and vertical (y) beam axis through the focus of a lens measured using a pyroelectric scanning slit beam profiler, with a Gaussian fit to the beam caustic.

discussed, this degradation is not surprising. The angular offset in the double-pass arrangement could also be contributing to this.

DISTRIBUTION A: Distribution approved for public release. Distribution unlimited

In conclusion, we have demonstrated the first CSP-based seeded OPG pumped by a Raman fiber amplifier at 1.24 µm. This is the first demonstration of MHz repetition rate pumping of CSP in the 1.2 µm region. Such a scheme allows the generation of widely tunable idler radiation in the 4.2–4.6 µm band, with idler powers of up to 0.25 W and total pump conversion efficiencies of 42%. Raman fiber lasers are available at custom wavelengths throughout the NIR with high peak and average powers, and we have demonstrated they can be paired with NCPM CSP-based parametric sources to create wavelength tunable light in the MIR. We also found that operating CSP at elevated temperatures can lead to an increased propensity for laser induced damage. This places a restriction on the tunability possible with NIR pumped CSP-based devices. More detailed studies are now required to fully understand the linear and nonlinear absorption of CSP at interesting Raman pump wavelengths in the 1–1.4µm region.

Novel parametric seeding architectures – cascaded four and three wave mixing

Summary

This work is a new area, aimed at high pulse energy picosecond sources at 2.94 µm for the precision ablation of biological tissue. Though the application lies outside the scope of this project, the underlying seeding architecture is a completely novel approach to seeding mid-infrared optical parametric amplifiers [24], [25]. This approach is shown in Figure 18.

One of the main technical requirements for all optical OPA systems is a seed, or signal, to amplify. By pumping optical fibers in the low normal dispersion region, it is possible to generate widely spaced, high power spectral density Stokes/anti-Stokes pulses through four-wave mixing (4WM). These pulses are inherently temporally and spatially overlapped with the pump pulse at the exit of the fiber, provided the walk-off length is long compared to the length of fiber employed. The output of the fiber can then be focused directly into a nonlinear crystal to convert the pump and Stokes/anti-Stokes pulses into the MIR through 3WM. Consequently, the need for additional signal beam delay and combination optics -commonly required in OPA and DFG systems - is avoided. By employing a fiber pump system, the 4WM stage could be fully fiber integrated with the pump, resulting in a compact, robust, and integrated pump system for the 3WM stage. This could ultimately lead to more user-friendly and field-deployable MIR sources, useful for a range of applications from surgery to remote sensing.

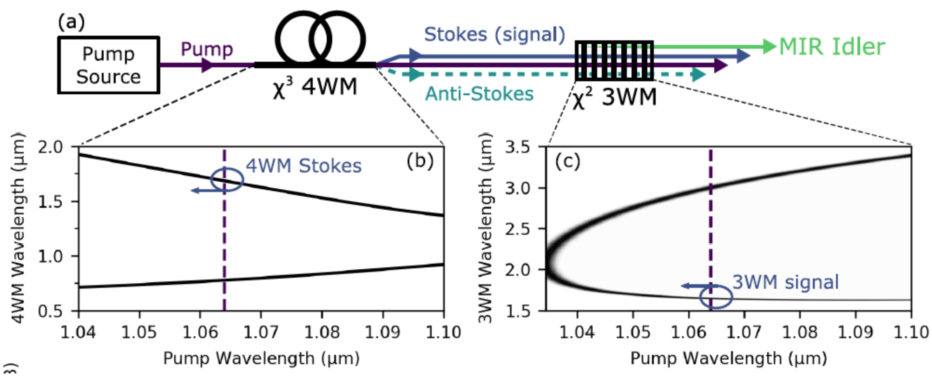

Figure 18 - (a) Schematic of MIR generation via cascaded $\chi^{(3)}$ four wave mixing (4WM) and $\chi^{(2)}$ three wave mixing (3WM). (b) Phase matching diagrams for the 4WM in PCF and (c) 3WM in PPLN (at 60°C).

DISTRIBUTION A: Distribution approved for public release. Distribution unlimited

Experimental results

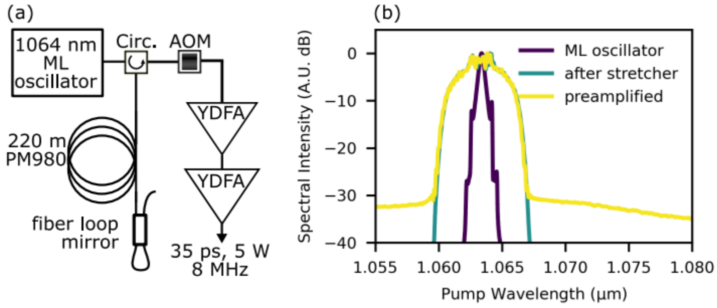

Figure 19 - Ytterbium fiber master oscillator power amplifier (MOPA) system. ML, mode-locked; Circ., Fiber circulator; AOM, acousto-optic modulator; YDFA, ytterbium-doped fiber amplifier. (b, c) Pump laser spectra at different positions along the MOPA chain.

We employed an Yb-fiber MOPA as the pump source, shown in Fig. 19(a). The MOPA system was constructed using polarization-maintaining components and seeded by a 50 MHz mode-locked Yb-fiber oscillator that produced 5 ps pulses. The seed pulses were stretched to 35 ps in a double pass of a 220 m length of polarization maintaining fiber (PM980), enabled through the use of a circulator and fiber loop mirror. The pulse stretching was essential to promote efficient four-wave mixing in the PCF conversion stage. An acousto-optic modulator was used to decrease the repetition rate by a factor of 1/6 to approximately 8 MHz and increase the achievable peak-power of the pump. Two stages of amplification were used to increase the average power to 5 W. The final stage amplifier was constructed from 2.8 m of ytterbium-doped fiber (Liekki Yb1200-10/125DC-PM) pumped by a wavelength stabilized 976 nm multimode diode. Residual 976 nm pump power was filtered from the collimated output of the MOPA using a short pass filter with a cut-on wavelength of 1000 nm. A free space optical isolator was used to prevent backreflections into the system, with a polarizing beam spliter and half wave plate providing power control.

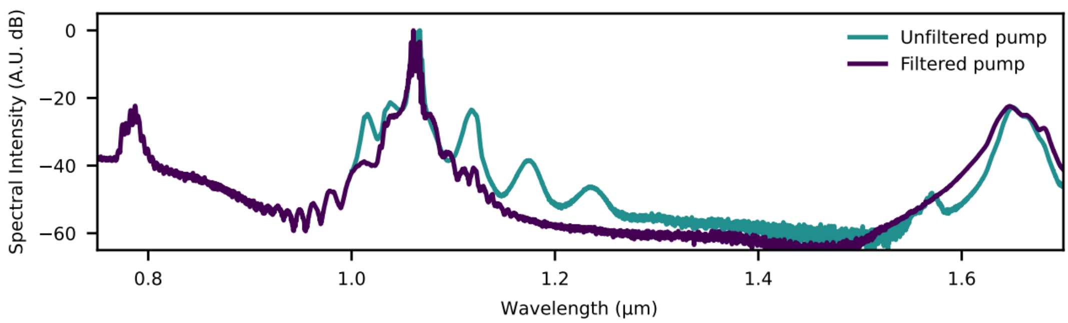

Figure 20 - Spectrum at output of PCF. With and without long pass 1100 nm filtering of the pump source to remove Raman scattered light.

The pump laser spectra at various points along and after the MOPA chain are shown in Fig. 19(b-c). The majority of the spectral broadening occurs in the stretching fiber, after which the 10 dB spectral width is 5.7 nm. The output spectra after the final stage of amplification remains centered around 1.064 μm with a 10 dB spectral width of 7.1 nm. A final filtering stage was implemented using a long

DISTRIBUTION A: Distribution approved for public release. Distribution unlimited

pass dichroic filter with a cut-on wavelength of 1100 nm to remove light around 1120 nm resulting from stimulated Raman scattering in the final amplifier stage, shown in Fig. 19(c).

The MOPA was used to pump a polarization-maintaining PCF. The PCF had zero dispersion wavelengths of 1.101 µm and 1.103 µm on the fast and slow axes respectively. The corresponding phasematching diagram for the slow axis of the PCF can be seen in Fig. 18(b). Spectral filtering to remove Raman shifted power in the pump spectrum, Fig. 19(c), was required before launching the pump into the PCF to prevent losses to further cascaded Raman shifts. Fig. 19 shows the output spectra of a 0.35 m length of PCF pumped on the slow axes with ≈ 3 W of coupled power, with and without 1100 nm long-pass Raman filtering before the PCF. FWM Stokes and anti-Stokes sidebands were generated in both cases, however without pre-filtering, significant power was transferred to the n = ±1, 2 Raman shifts (n × 13.2 THz in silica) from the pump.

The Stokes and anti-Stokes sidebands generated by FWM in the PCF depended on the pump polarisation relative to the PCF fast and slow axes. Fig. 21(a) demonstrates the effect of rotating the launched pump polarisation on the generated Stokes spectra for a coupled pump power of approximately 3 W. As the pump polarisation was rotated, the two distinct axes can be easily identified by the change in generated Stokes wavelength. For intermediate launched pump polarisations which did not align with either axes, the Stokes spectral intensity and width was reduced. When the launched pump polarization state was orientated at 45° to each of the axes of the fiber, sidebands corresponding to both the fast and slow axes could be observed. The shift in the Stokes spectrum as a function of pump power is shown in Fig. 21(b) for coupled pump powers between 2-3 W launched on the slow-axis. The peak Stokes wavelength decreased as the coupled pump power increased and significant Stokes spectral broadening was observed.

The output of the PCF was focused directly into a PPLN crystal doped with 5 mol.% MgO (HC Photonics). The PPLN crystal had a poling period of 31.3 µm, and dimensions 3x3x10 mm3 . Numerous lenses of varying focal length were investigated when optimising focusing into the crystal. The overlap of the pump and Stokes beams after focusing was investigated using a scanning slit beam profiler. To measure the signal beam diameters, a long pass 1300 nm filter at an angle of 45° was used between the PCF collimating lens and the focussing lens.

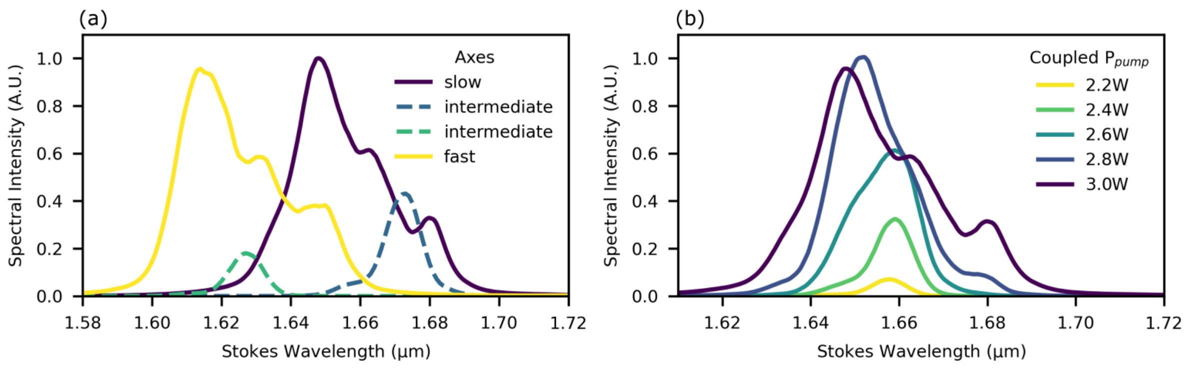

Figure 21 - (a) Generated Stokes sidebands on the fast and slow axes, and at intermediate positions between the principle axes. (b) Generated Stokes sidebands variation with coupled pump power on the fast axes.

The greatest MIR idler generation was observed for the shortest focal length focusing lens and hence the greatest pump and signal intensity in the crystal. The crystal oven size physically limited the

DISTRIBUTION A: Distribution approved for public release. Distribution unlimited

shortest possible focal length lens to 35 mm. At this focal length, the Rayleigh range of the pump in free-space (approximately 0.7 mm) was much shorter than the crystal length (10 mm).

Tuning the crystal temperature in the range 40-100°C resulted in tuning of the idler spectra as shown in Fig. 22 (a). The associated variation in the generated idler and amplified signal powers is shown in Fig. 22 (b). The phase matched signal wavelength increases with temperature for a fixed pump wavelength. The peak wavelength of the generated idler therefore decreased as the crystal temperature was increased. At a temperature of 120°C, the seed signal was no longer phase matched, and no idler power was generated. This confirmed that the FWM Stokes pulses were seeding the MIR generation. A maximum 115 mW of generated idler at around 3 μm alongside 189 mW of amplified signal were generated at a crystal temperature of 60°C.

We have demonstrated a new method of generating MIR pulses by cascading χ (3) FWM in fiber and χ (2) OPA/DFG in a nonlinear crystal. The simple architecture utilizes the inherent spatial and temporal overlap of pulses generated by FWM in fiber to both pump and seed the OPA/DFG. We use this technique to generate MIR light at around 3 μm, a useful wavelength for tissue ablation applications. Ongoing investigations and simulations aim to determine the limits of the conversion efficiency into the MIR using this architecture.

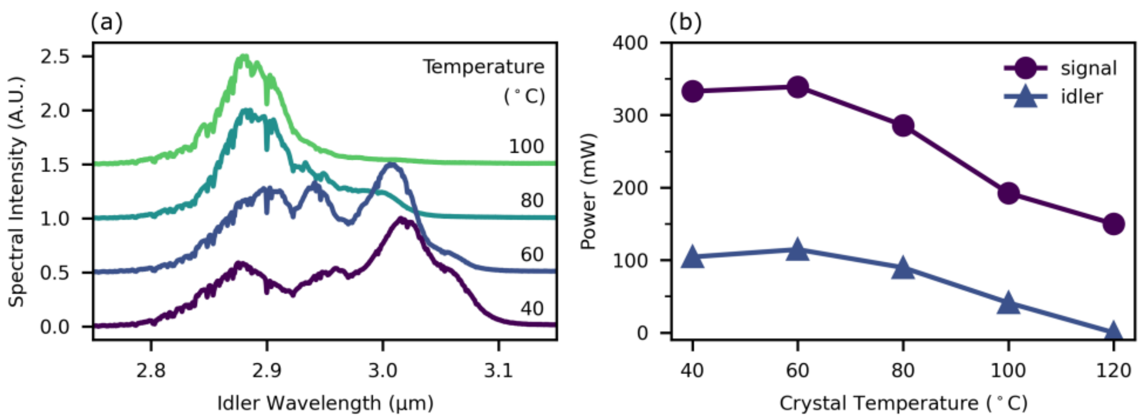

Figure 22 - (a) Idler wavelength tuning with temperature. (b) Generated idler and amplified signal power tuning with temperature.

Report references

[1] R. T. Murray, T. H. Runcorn, S. Guha, and J. R. Taylor, "High average power parametric wavelength conversion at 3.31-3.48 μm in MgO:PPLN," *Opt. Express*, vol. 25, no. 6, pp. 343–348, 2017, [Online]. Available: https://www.osapublishing.org/oe/abstract.cfm?uri=oe-25-6-6421.

[2] R. T. Murray, T. H. Runcorn, S. Guha, and J. R. Taylor, "Fibre MOPA Pumped MIR Parametric Wavelength Conversion [Invited]," in *Laser Congress 2017 (ASSL, LAC)*, Oct. 2017, p. AM2A.1, doi: 10.1364/ASSL.2017.AM2A.1.

[3] S. Guha, P. G. Schunemann, K. T. Zawilski, and R. T. Murray, "Mid-Infrared Generation Through Nonlinear Frequency Conversion Processes [Invited]," 2017.

[4] R. T. Murray, "Fibre laser pumped optical parametric amplifiers in the mid-infrared [Invited]," 2017.

[5] R. T. Murray, T. H. Runcorn, and J. R. Taylor, "Fibre-based Sources from the UV to Mid-Infrared," in *Advanced Photonics Congress 2018 (BGPP, IPR, NP, NOMA, Sensors, Networks, SPPCom,*

DISTRIBUTION A: Distribution approved for public release. Distribution unlimited

SOF), Jul. 2018, p. SoTu3G.1, doi: 10.1364/SOF.2018.SoTu3G.1.

[6] R. T. Murray, T. H. Runcorn, S. Guha, and J. R. Taylor, "Fibre MOPA pumped MIR parametric wavelength conversion (Conference Presentation) [Invited]," in *Proc. SPIE 10516, Nonlinear Frequency Generation and Conversion: Materials and Devices XVII*, 2018, pp. 10516–12, doi: https://doi.org/10.1117/12.2295112.

[7] R. T. Murray, T. H. Runcorn, E. J. R. Kelleher, and J. R. Taylor, "Highly efficient mid-infrared difference-frequency generation using synchronously pulsed fiber lasers," *Opt. Lett.*, vol. 41, no. 11, pp. 2446–2449, May 2016, doi: 10.1364/OL.41.002446.

[8] L. Xu, H.-Y. Chan, S. Alam, J. D. Richardson, and P. D. Shepherd, "High-energy, near-and mid-IR picosecond pulses generated by a fiber-MOPA-pumped optical parametric generator and amplifier," *Opt. Express*, vol. 23, pp. 12613–12618, 2015, [Online]. Available: http://www.osapublishing.org/abstract.cfm?uri=oe-23-10-12613.

[9] P. Belden, D. Chen, and D. F. Teodoro, "Watt-level, gigahertz-linewidth difference-frequency generation in PPLN pumped by an nanosecond-pulse fiber laser source," *Opt. Lett.*, vol. 40, pp. 958–961, 2015, [Online]. Available: http://www.osapublishing.org/ol/fulltext.cfm?uri=ol-40-6-958.

[10] Y. Peng *et al.*, "High-power and widely tunable mid-infrared optical parametric amplification based on PPMgLN.," *Opt. Lett.*, vol. 41, no. 1, pp. 49–51, Jan. 2016, doi: 10.1364/OL.41.000049.

[11] G. Arisholm, R. Paschotta, and T. Sudmeyer, "Limits to the power scalability of high-gain optical parametric oscillators and amplifiers," in *Conference on Lasers and Electro-Optics Europe - Technical Digest*, Mar. 2003, vol. 21, no. 3, p. 262, doi: 10.1109/CLEOE.2003.1312323.

[12] A. M. Chandran, T. H. Runcorn, R. T. Murray, and J. R. Taylor, "Nanosecond pulsed 620 nm source by frequency-doubling a phosphosilicate Raman fiber amplifier," *Opt. Lett.*, vol. 44, no. 24, pp. 6025–6028, 2019.

[13] A. M. Chandran, T. H. Runcorn, R. T. Murray, and J. R. Taylor, "620 nm source by second harmonic generation of a phosphosilicate Raman fiber amplifier," in *Conference on Lasers and Electro-Optics, Technical Digest Series (OSA Publishing Group, 2019)*, 2019, p. SM3L.4, doi: 10.1364/CLEO_SI.2019.SM3L.4.

[14] T. H. Runcorn, F. Gorlitz, R. T. Murray, and E. J. R. Kelleher, "Visible Raman-shifted Fiber Lasers for Biophotonic Applications," *IEEE J. Sel. Top. Quantum Electron.*, vol. 24, no. 3, 2018, doi: 10.1109/JSTQE.2017.2770101.

[15] S. M. Riecke *et al.*, "Picosecond Spectral Dynamics of Gain-Switched DFB Lasers," *IEEE J. Quantum Electron.*, vol. 47, no. 5, pp. 715–722, May 2011, doi: 10.1109/JQE.2010.2096501.

[16] R. T. Murray *et al.*, "CdSiP2 based mid-infrared optical parametric sources pumped with Raman fiber amplifiers," in *Advanced Photonics Congress 2021 (IPR, Networks, NOMA, PVLED, SPPCom)*, 2021, p. NoW2A.1, doi: 10.1364/noma.2021.now2a.1.

[17] R. T. Murray *et al.*, "Seeded optical parametric generation in CdSiP2 pumped by a nanosecond pulsed, MHz repetition rate Raman fiber amplifier at 1.24 µm," in *Proc. SPIE 11670, Nonlinear Frequency Generation and Conversion: Materials and Devices XX*, Mar. 2021, vol. 11670, p. 6, doi: 10.1117/12.2582686.

[18] R. T. Murray *et al.*, "Seeded optical parametric generation in CdSiP2 pumped by a Raman fiber amplifier at 1.24 µm," *Opt. Lett.*, vol. 46, no. 9, pp. 2039–2042, May 2021, doi: 10.1364/OL.420959.

DISTRIBUTION A: Distribution approved for public release. Distribution unlimited

[19] R. T. Murray, J. Anderson, J. Wei, K. T. Zawilski, P. G. Schunemann, and S. Guha, "Wavelength tunable mid-infrared generation in non-critically cut CdSiP2 crystals by cascaded optical parametric generation with a nanosecond 1.064 µm Nd:YAG laser," in *Conference on Lasers and Electro-Optics, Technical Digest Series (Optica Publishing Group, 2022)*, 2022, p. SM2O.2.

[20] A. Hildenbrand-Dhollande *et al.*, "Laser-Induced Damage Study at 1.064 and 2.09 µm of High Optical Quality CdSiP2 Crystal," in *Advanced Solid State Lasers*, Oct. 2015, p. AM2A.8, doi: 10.1364/ASSL.2015.AM2A.8.

[21] S. Chaitanya Kumar, K. T. Zawilski, P. G. Schunemann, and M. Ebrahim-Zadeh, "High-repetition-rate, deep-infrared, picosecond optical parametric oscillator based on CdSiP_2," *Opt. Lett.*, vol. 42, no. 18, p. 3606, Sep. 2017, doi: 10.1364/ol.42.003606.

[22] V. Kemlin *et al.*, "Nonlinear, dispersive, and phase-matching properties of the new chalcopyrite CdSiP_2 [Invited]," *Opt. Mater. Express*, vol. 1, no. 7, p. 1292, Nov. 2011, doi: 10.1364/ome.1.001292.

[23] J. Wei *et al.*, "Measurement of refractive indices of CdSiP_2 at temperatures from 90 to 450 K," *Opt. Mater. Express*, vol. 8, no. 2, p. 235, Feb. 2018, doi: 10.1364/OME.8.000235.

[24] R. A. Battle *et al.*, "Optical parametric amplification seeded by four-wave mixing in photonic crystal fibers," in *Proc. SPIE 11985, Nonlinear Frequency Generation and Conversion: Materials and Devices XXI*, 2022, vol. 1198502, no. March, p. 4, doi: 10.1117/12.2609618.

[25] R. A. Battle *et al.*, "Mid-infrared parametric wavelength conversion seeded with fiber optical parametric sources," in *EPJ Web of Conferences, EOSAM 2021*, 2021, vol. 255, p. 11004, doi: 10.1051/epjconf/202125511004.

DISTRIBUTION A: Distribution approved for public release. Distribution unlimited